

**CGMS  
IPWG**



*International Precipitation  
Working Group*



**P  
r  
o  
c  
e  
e  
d  
i  
n  
g  
s**



## **1st Workshop**

**Madrid, Spain**

**23-27 September 2002**



**EUMETSAT**

# VALIDATION OF AN OPERATIONAL GLOBAL PRECIPITATION ANALYSIS AT SHORT TIME SCALES

F. Joseph Turk<sup>1</sup>, Elizabeth E. Ebert<sup>2</sup>, Hyun-Jong Oh<sup>3</sup>, Byung-Ju Sohn<sup>3</sup>, Vincenzo Levizzani<sup>4</sup>, Eric A. Smith<sup>5</sup>, and Ralph Ferraro<sup>6</sup>

## Abstract

In order to properly utilize meteorological satellite-derived precipitation estimates in operational settings such as numerical weather prediction (NWP) applications, knowledge of the observation error statistics are needed as well as information how they are correlated in space and time. However, very few raingauge networks operate with the necessary spatial density and time resolution required for validation of a satellite-based precipitation analysis generated at the required space and time scales (e.g., 0.25-degree or less and sub-six-hourly). We examine over-land validation statistics for an operationally designed, global rainfall analysis that blends intermittent passive microwave (PMW)-derived rainfall estimates aboard a variety of low Earth-orbiting (LEO) satellite platforms with sub-hourly time sampling capabilities available from thermal infrared (IR) imagers aboard operational geostationary platforms. The blended satellite analysis is formulated upon area-dependent statistical relationships derived from a precise, near real time ensemble of orbit-intersecting PMW and IR pixels from a constellation of LEO and geostationary satellites, respectively. Using the dense, nearly homogeneous, one-minute reporting Automated Weather Station (AWS) raingauge network of the Korean Meteorological Agency (KMA) during June-August 2000, the space-time RMS error, mean bias, and correlation matrices were computed using various time windows for the gauge averaging, centered about the satellite observation time. For +/-10-minute time window, a correlation of 0.6 was achieved at 0.1-degree spatial scale by averaging over 3 days; coarsening the spatial scale to 1.8 degrees produced the same correlation by averaging over one hour. Finer than approximately 24-hours and 1-degree time and space scales, respectively, a rapid decay of the error statistics was obtained by trading off either spatial or time resolution. Beyond 24-hours time scale, the blended estimates were nearly unbiased and with an RMS error of no worse than 1 mm d<sup>-1</sup>. Using the 0.25-degree resolution Australian Bureau of Meteorology (BOM) daily raingauge analysis, the blended technique estimate and a separate, merged PMW-only rain estimate were validated over one year beginning in April 2001. The blended technique clearly performed best in the wet season and the tropical latitudes and had difficulty capturing mid-latitude winter season frontal rain systems. The overall error characteristics of the blended satellite technique appear to be limited by the worst-case revisit time of the underlying LEO constellation, which remains at about six hours in the tropics. Also, the results suggest that the performance of this type of blended satellite technique may be more sensitive to inter-satellite relative biases between the PMW sensor types than by gaps in the intermittent time sampling pattern of the underlying LEO constellation.

## 1. Introduction

---

<sup>1</sup> Marine Meteorology Division, Naval Research Laboratory, Monterey, CA 93943, USA

<sup>2</sup> Weather Forecasting Group, Bureau of Meteorology Research Centre, Melbourne, Victoria 3001, Australia

<sup>3</sup> School of Earth and Environmental Sciences, Seoul National University, Seoul 151-742, Korea

<sup>4</sup> CNR-Institute of Atmospheric Sciences and Climate, Via Gobetti 101, I-40129, Bologna, Italy

<sup>5</sup> NASA Goddard Space Flight Center, Greenbelt, MD 20771, USA

<sup>6</sup> NOAA-NESDIS, Camp Springs, Maryland 20746, USA

The past two decades have witnessed the rapid evolution of the low Earth-orbiting (LEO) passive microwave (PMW) imaging sensor from a research setting into routine operational settings. The conically-scanning, sun-synchronous orbiting Special Sensor Microwave Imager (SSM/I) imagers onboard the Defense Meteorological Satellite Program (DMSP) satellites launched between 1987 and 1999 were joined by the joint United States/Japan Tropical Rainfall Measuring Mission (TRMM) Microwave Imager (TMI) in 1997 (Kummerow et. al., 1998, 2000), and the Advanced Microwave Scanning Radiometer (AMSR-E) aboard the Earth Observing System (EOS) Aqua in 2002. The spatial resolution of the instantaneous precipitation estimate derived from these sensors is primarily determined by the diffraction-limited, coarser field-of-view (FOV) low frequency, emission-based window channels (10-19 GHz) in the over-ocean situation, and from the narrower FOV, higher frequency, primarily scattering-based channels (37-85 GHz) over land (Spencer et. al., 1989). A variety of conditions make precipitation problematic to validate. The changing time and three-dimensional spatial scales of global precipitation processes, the intermittent and unequally spaced satellite revisit (i.e. the time between successive overpasses), the instantaneous nature of a moving-platform satellite observation, the characteristics of the validation system, among others, each effect must be considered in order to properly derive and interpret validation statistics. To attempt to validate a satellite-based precipitation analysis at a daily or sub-daily time scale and a sub-degree spatial scale requires a validation system with a dense, homogeneous spatial coverage and a time sampling rate fast enough (and extended over a long enough period of time) to coordinate meaningful comparisons with the instantaneous nature of moving-platform satellite-based observations, and some means to supplement (or account for) the intermittent LEO overpass schedule.

Increasingly, the need and future planning for various sub-daily time and sub-degree space scale global precipitation products has gained prominence, largely driven by hydrological and Numerical Weather Prediction (NWP) improvements and applications. For example, a typically quoted goal of the proposed Global Precipitation Mission (GPM) is to collect sufficient instantaneous observations from a constellation of LEO platforms over a time window sufficient to avoid diurnal aliasing (typically three hours or less), with a 0.1-degree global resolution (Fleming, 2002). The Advanced Microwave Sounding Unit-B (AMSU-B), an across-track scanning humidity sounder onboard the National Oceanic and Atmospheric Administration (NOAA) operational LEO satellites, has an operational rainfall product which is distributed by the National Environmental Satellite Data Information Service (NESDIS) Microwave Surface and Precipitation Products System (MSPPS) (Weng et al., 2002). Overall, when all of the above-mentioned LEO satellite platforms are taken into account (three DMSP, one TMI, and three NOAA as of autumn 2002), orbit calculations show that the resultant worst-case revisit still hovers near six hours in the tropical latitudes.

With the fundamental intermittent nature of PMW observations, the idea of capitalizing on the frequent, routinely scheduled infrared (IR) observations available from geostationary operational meteorological satellite platforms has received increasing attention in recent years, especially since the deployment of the first of the Geostationary Orbiting Earth Satellite (GOES) I-M imagers in 1994. The idea behind combining these sensor types was investigated soon after the public availability of the DMSP SSM/I data in the early 1990s (Adler et.al., 1993; Vicente, 1994; Levizzani et.al., 1996) and has continued with other varied efforts (Kidd et.al., 1998; Miller et.al., 2000; Todd et.al., 2001; Morales and Anagnostou, 2002; Adamo et al., 2002; Grecu et al., 2000; Ba et al., 2001). In August 2002, the first of the Meteosat Next Generation (MSG) geostationary platforms was successfully launched, carrying as its core instrument the Spinning Enhanced Visual and Infrared Imager (SEVIRI), a 12-channel imager. (Schmetz et. Al., 2002). As part of its Fifth Framework Program, the European Commission (EC) has funded the EURAINSAT program, which is developing (among others) a blended SEVIRI-PMW rainfall technique (Levizzani et al., 2002) as its core rainfall algorithm to assimilate rainfall into mesoscale forecast systems and to provide timely data to civil protection agencies. Here, we define a blended satellite technique as a method which joins together direct (PMW-based rainfall observations) and indirect (brightness temperatures from IR sensors) datasets, gathered at different space and time scales, under a scale transformation and normalization process to produce a final rainfall product. The blended

technique described in this article was initially developed in 1998 at the Naval Research Laboratory (NRL) in an effort to improve upon 2-3 day hurricane track forecasting (Turk et al., 2000). While the core of the technique has been improved somewhat since then (to 3-hourly and 0.1-degree), and used in several applications (Krishnamurti et al., 2001; Grose et al., 2002), it has never undergone a thorough validation.

This article focuses specifically upon validation and performance of the NRL blended technique at various space and time scale combinations, using raingauge data from two rain gauge networks, the densely spaced, 1-minute reporting Korean Meteorological Administration (KMA) Automated Weather Station (AWS) network and the daily analysis produced by Australian Bureau of Meteorology (BOM) continental raingauge system. The need for validation at various space/time scales is driven by NWP model requirements, where precipitation is a diagnosed quantity (rather than a prognostic one), and various assimilation techniques have been developed which handle precipitation data. Variational data assimilation systems require knowledge of the precipitation estimation uncertainty and how it is correlated in space and time (Bauer et al., 2002). The error covariances between the rainfall observations and the model background field determine how the observation data is allowed in the model analysis. To attempt to characterize the precipitation analysis requires a validation system with a dense, homogeneous spatial coverage and a time sampling rate large enough (and extended over a long enough period of time) to permit meaningful comparisons with the instantaneous nature of moving-platform satellite-based observations. The AWS data was averaged to various combinations of sub-daily and sub-1-degree space and time scales in order to minimize, but not totally account for, fundamental discrepancies between a satellite-based and a raingauge-based observation (Oh et al., 2002) and presents, as a first attempt, a means to produce estimates of fine spatial scale and short time scale satellite-derived precipitation error statistics.

## 2. Blended technique description

In order to blend the disjoint LEO PMW and geostationary IR measurements in an automated and adaptive manner, the blended technique starts by subdividing the Earth into a 2-degree/pixel grid (60 lines by 180 samples) with a finer, 0.25-degree/pixel grid (480 lines x 1440 samples) nested inside it (the reason for these values are discussed below) between 60N and 60S. As new PMW datasets arrive, currently one orbit per satellite, the PMW-derived rainrate pixels are paired with their time and space-coincident geostationary 11-  $\mu\text{m}$  IR brightness temperature ( $T_B$ ) data, using a 15-minute maximum allowed time offset (denoted by  $\Delta t$ ) between the pixel observation times and a 10-km maximum allowed spatial offset (denoted by  $\Delta d$ ) as depicted in Fig. 1.

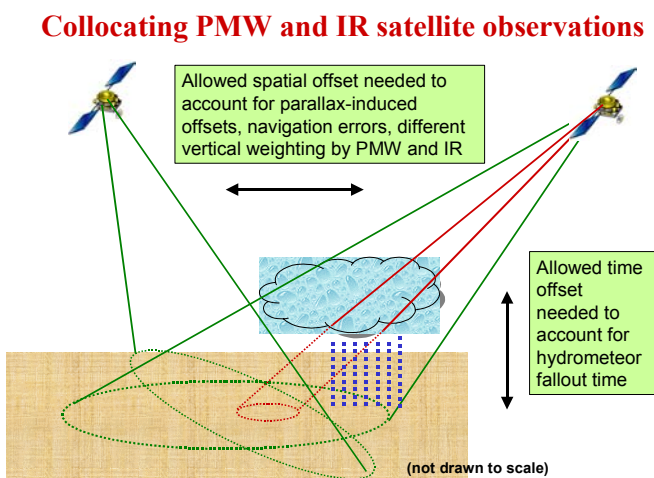


Figure 1. Some factors influencing the necessity averaging to account for spatial and temporal offsets, when aligning geostationary IR and LEO PMW datasets on a per-pixel basis.

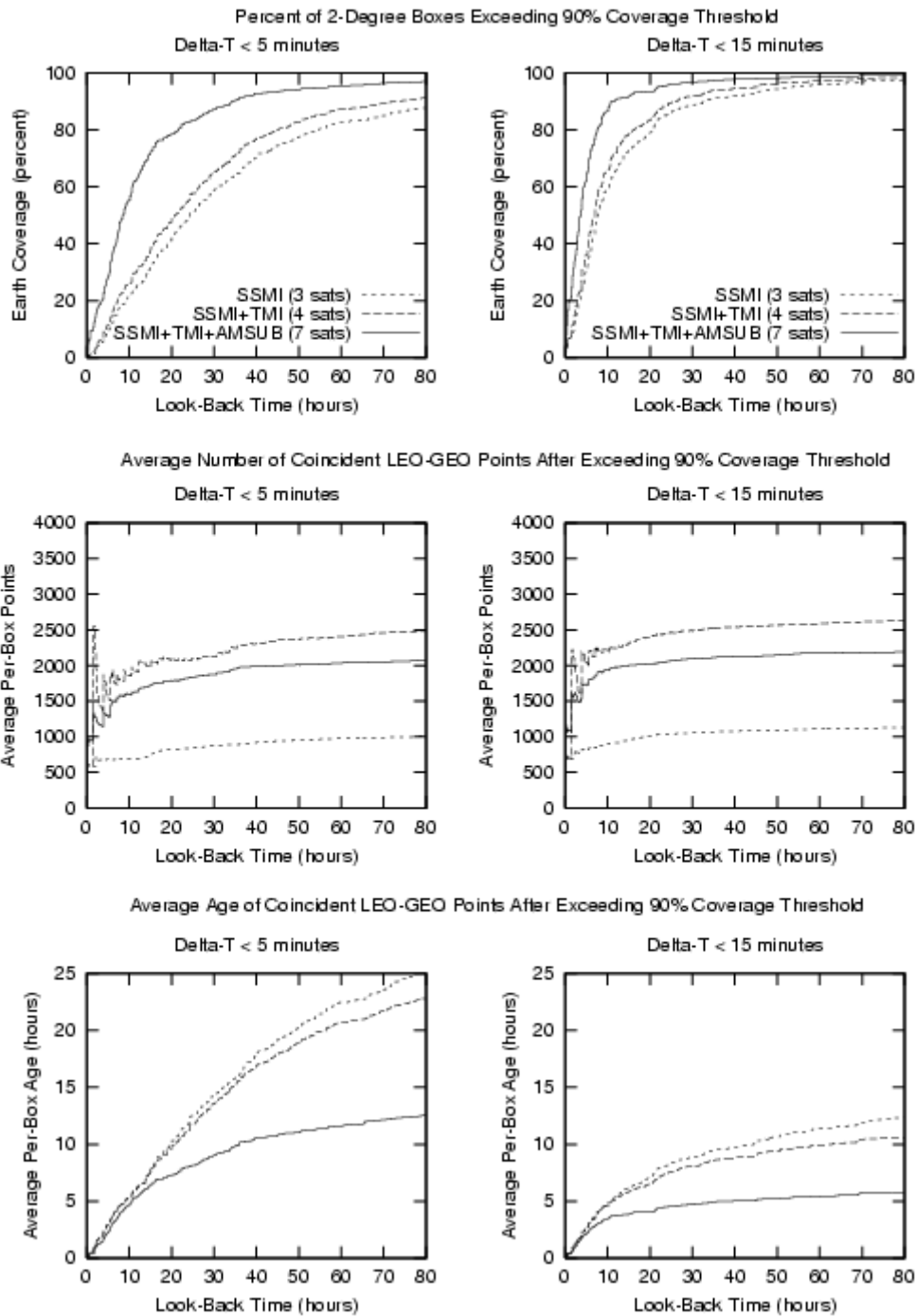


Figure 2. **Left side:** (a) Percentage of 2-degree boxes covered with time/space coincident IR-PMW observations over the Earth from 60S-60N latitude, as a function of the look-back time, and the number and type of Low Earth Orbiting (LEO) satellite sensors used. The look-back time begins at 09 UTC on 3 October 2002 and runs backwards. (b) Average number coincident observations in each 2-degree box. (c) Average age in hours of the coincident observations in each 2-degree box. The maximum allowed time and space offsets between the LEO-based microwave sensor pixel and the geostationary IR pixel are 5 minutes and 10 km, respectively. **Right side:** Same as left side panels, but for a maximum allowed time offset between the LEO-based microwave sensor pixel and the geostationary IR pixel of 15 minutes.

Prior to this, the geostationary data are averaged to the approximate resolution of the PMW rainfall datasets (30-km for SSM/I, 10-km for TMI, and between 15-50 km for AMSU-B depending upon scan position), and parallax-induced geolocation displacements are accounted for using the procedure of Vicente et al. (2002). Each collocated data increments histograms of the IR  $T_B$  and the PMW rain rate in the nearest  $2^\circ$  box, as well as the eight surrounding boxes (this overlap assures a fairly smooth transition in the histogram slopes between neighboring boxes). As soon as a  $2^\circ$  box is refreshed with new LEO data, a probabilistic histogram matching relationship (Calheiros and Zawadski, 1987) is updated using the PMW rainrate and IR  $T_B$  histograms, and a  $T_B$ -R lookup table is created. To assure that the most timely rain history is maintained, the histograms of these coincident data are accumulated backwards from the current clock time (the "look-back" time) until the spatial coverage of a given 2-degree box exceeds a 90 percent coverage threshold (the inner 0.25-km/pixel mesh is fine enough to enable an approximation of the percent coverage).

Fig. 2 shows the overall percentage of 2-degree boxes that reach this coverage threshold as a function of the look-back time and the type of LEO satellites used in the coincident pixel alignment procedure. The addition of the three AMSU-B instruments to the three SSM/Is and the TMI (7 satellites, dotted line) permits 90% of the Earth between 60S-60N latitude to be covered with coincident data observations within 15 hours of look-back time, with an average of about 2000 coincident observations per box. With three SSM/Is and the TMI (4 satellites, dashed line), the same total Earth coverage is reached after 30 hours, but with an average of 2500 coincident observations per 2-degree box (this is due to the fact that the AMSU-B data are coarser than the TMI, and although they may arrive prior to the TMI data, they are less in number). The bottom panel demonstrates that for 90 percent Earth coverage, the average age of the data in each 2-degree box is about 4 hours when the 7-satellite combination is used, significantly shorter than the 8-hours in the 4-satellites case and 10-hours in the SSM/I-only (3 satellites) case. For comparison, Fig. 2 also illustrates these same statistics, but with a smaller maximum allowed  $\Delta t=5$  minutes. Under these circumstances, it takes about 35 hours to achieve the 90% Earth coverage for the 7-satellite case and the average age of these data are about 10 hours. While the smaller time offset is preferred in order to capture as nearly time-coincident data as possible, with the current 7-satellite configuration it comes with the expense of increased age of coincident data observations. With this inherent tradeoff in mind, all results discussed hereafter used  $\Delta t=15$  minutes and  $\Delta d=10$  km in the PMW-IR coincident data alignment procedure.

This lookup table update process is constantly ongoing with operationally arriving LEO and geostationary data. The transfer of this information to the stream of steadily arriving geostationary data is then a relatively simple lookup table procedure. For each newly arrived geostationary dataset, the IR channels are map-registered onto a global, 0.1-degree rectangular map projection for all pixels whose satellite zenith angle is less than 70 degrees. For each 0.1-degree pixel, the closest 2-degree histogram box and the eight surrounding boxes are located, and an inverse-distance weighted average is computed from these nine lookup table-derived rainrates (this minimizes discontinuities across histogram box boundaries). Lastly, NWP forecast model 850 hPa wind vectors from an NWP forecast model are combined with a 2-minute topographic database, and a correction is applied in regions of likely orographic enhancement, following the formulation of Vicente et al. (2002). The use of a common 0.1-degree global map projection for all geostationary satellites greatly speeds up the computation of rainfall accumulations, and compensates for the coarser resolution of geostationary IR data at higher latitudes. At specified synoptic time intervals (usually every three hours), the rainfall accumulations are updated as far back in time as desired by backwards time-integrating.

The blended satellite technique is autonomous and self-adapting, and the adjustable parameters are the histogram box size, allowable pixel collocation time and space offsets ( $\Delta t$  and  $\Delta d$ , respectively), and minimum spatial coverage of each box required to initiate its lookup table update. As additional LEO satellites are added to the blending procedure, presumably the histogram box size and allowable space/time offsets can be made smaller, which should better capture individual smaller-scale rainfall systems, although this remains to be examined when data

from upcoming LEO platforms are available. In operational settings, one or more LEO datasets may be missing or arrive later than a data cutoff time. To limit this, we set a maximum look-back time of 24-hours, which may temporarily disable the blended technique over certain parts of the Earth where the overall LEO revisit time is the longest. Currently, visible data are not used in this technique since we have not yet sufficiently examined how they can be seamlessly used across the day-night terminator. We have resorted to using only the common 11- $\mu\text{m}$  channel at this point since it is common to all current geostationary satellites, but other formulations should be used to relate the PMW and IR data to take full advantage of the expanded thermal and solar spectral capabilities offered in the MSG and GOES-R series of geostationary satellites. Already, Marzano et al. (2002) have tested multivariate probability matching and nonlinear multiple regression techniques for the PMW-IR blending. We are currently examining the use of the Moderate Resolution Imaging Spectrometer (MODIS) 6.7  $\mu\text{m}$  water vapor channel in combination with its 11- $\mu\text{m}$  in order to retrieve information when the cloud top is near or above the tropopause. While the technique may seem computationally burdensome, we note that we process all 12 (currently 7 LEO and 5 GEO) satellites and the 3-hourly interval accumulation updates (run out to 72-hours) on a single dual-processor Linux-based PC.

### 3. Validation with the KMA AWS network

The Korean Meteorological Agency (KMA) maintains an operational, densely spaced Automated Weather Station (AWS) over the southern Korean Peninsula, consisting of nearly 500 tipping-bucket, uniformly-spaced, one-minute updating rain gauges (approximately 40 gauges per 1-degree box). Fig. 3 depicts the AWS grid (not all stations are plotted).

One Minute Raingage Network over Korea

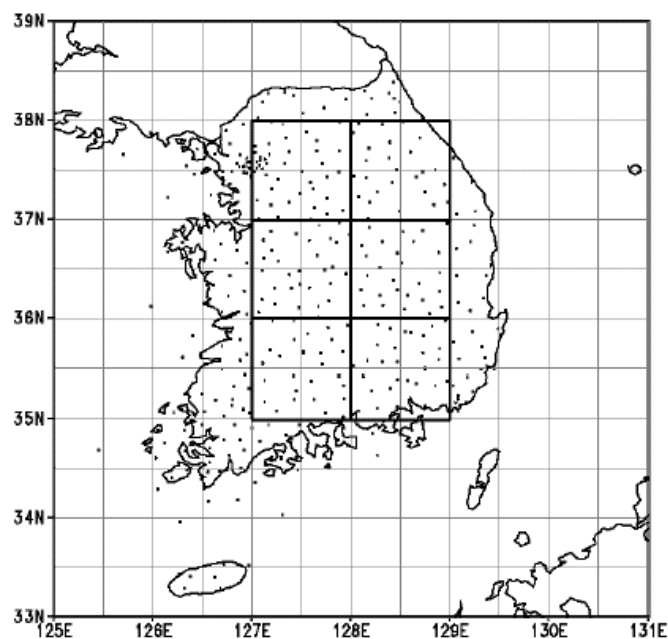


Figure 3. Depiction of the Automated Weather Station (AWS) operational rain gauge network, operated by the Korean Meteorological Agency. The density is nearly homogeneous across the southern Korean peninsula with 40 gauges per 1-degree box, each reporting at a 1-minute time update resolution.

AWS data were collected during June-August 2000 along with the individual hourly, instantaneous rainfall datasets produced by the blended satellite technique (the GMS-5 satellite is the only

geostationary satellite that provides coverage and its refresh rate is hourly beginning at 30 minutes after each hour, and the Korean Peninsula is imaged about 8 minutes after the frame start time). Fig. 4 depicts the shaded color maps of the mean monthly rainrate over the Southern Korean peninsula during June, July and August 2000.

### Monthly Mean of Rainrate (2000)

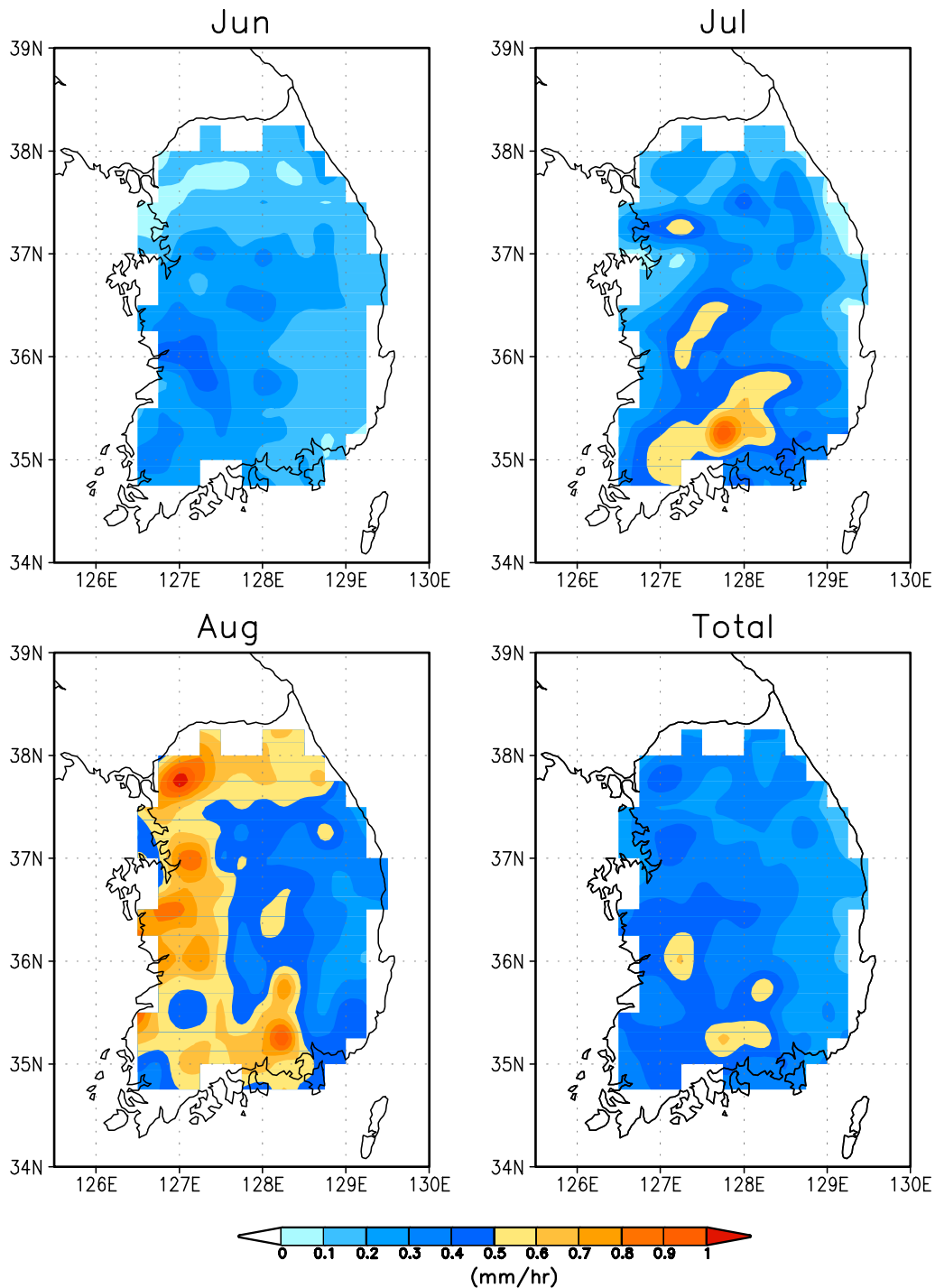


Figure 4. Maps of the monthly mean rainrate over the South Korean peninsula for June, July and August 2000.

During this time, the NOAA-15/16/17 satellites were not yet incorporated into the blended technique (the three SSM/Is and the TMI formed the underlying LEO constellation), giving a LEO revisit over Korea of about 4 hours on average and 10 hours worst-case. Considering that an individual satellite observation represents an approximate 0.1-degree area average, whereas the gauge measurement represents a small area less than 1 m<sup>2</sup>, South Korea is divided into smaller boxes, ranging from 0.1 degrees to 3 degrees on a side, where relatively homogeneous gauge distributions are found (Fig. 3 depicts the 1-degree box size). Due to the inhomogeneity of the rain within the spatial averaging box and very small areas represented by individual gauges, a direct comparison of instantaneous (ie, pixel-based) satellite-based retrievals and gauges is inherently limited. For intermittent and sporadic rain events, the rain may fall between but not into individual gauges, or the rainfall pattern may evolve and move between the gauge locations. Using the AWS network and various IR-based rainfall techniques over a one-month period, Oh et al (2002) investigated the impact of the spatial rain inhomogeneity by analyzing the number of rain-detected gauges in individual 1-degree boxes. They found that the satellite algorithm validation was more likely to fail for sporadic and weak rain events when the number of rain-detecting gauges per 1-degree box was less than 15. However, in some cases, isolated convective rain events may be characterized by a small number of rain-detecting gauges, so a simple minimum-gauge criterion is not necessarily sufficient in all cases. In the discussion to follow, it must be therefore be remembered that unambiguous interpretation is not always possible with gauge-satellite comparisons, especially for sporadic rain events.

The instantaneous estimate from the blended satellite technique essentially consists of transferring the past-time PMW-IR history (via the lookup tables) to newly gathered IR radiances, whose information content originates at or near the physical cloud top height, whereas the gauge data is a purely ground-based observation. Therefore, to account for the fallout time of the hydrometeors, the gauge data were first averaged over time windows varying between +/-1 to +/-30 minutes, centered about the AMSR-2 observation time. Then, at each spatial resolution, these data were time-integrated over various time intervals ranging from one hour (the minimum time interval) to 30 days. That is, the original data were fixed at one spatial scale and then integrated over the various time scales, then repeated for the next spatial scale, and so on. This allows the blended technique validation to be performed in a two-dimensional, space-time fashion. Most importantly, the 1-minute time resolution of the KMA network allows individual, instantaneous satellite pixels to be paired in time with the corresponding rain gauge pixels prior to any temporal averaging.

For example, Fig. 5 shows the scatter plots of the blended satellite ( $R_S$ ) vs. gauge ( $R_G$ ) comparison at a 1-degree spatial scale and for six time scales ranging from 1-hour to 24-hours, where the AMSR-2-GMS time window was fixed at +/-10 minutes. As expected, the correlation improves with longer time averaging, but the bias remains near zero or slightly negative, with a large variance. The 24-hour plot demonstrates that when  $R_G < 1 \text{ mm h}^{-1}$ , the blended technique often assigned light rain to regions where  $R_G = 0$ . While it is difficult to unravel an exact cause of these characteristics, it is possible that this is related to the PMW algorithm rain/no-rain screening. Over land, the NESDIS operational SSM/I algorithm is used in the Version-5 TMI 2A12 rainfall algorithm (Kummerow et al., 2001). Under certain conditions, light rain can be misidentified over a variety of Earth surfaces that appear to scatter radiation similar to a precipitating cloud (Bauer et al, 2000; Conner and Petty, 1998; Ferraro et al., 1998). In the automated histogram matching procedure, these (falsely-identified) light rain pixels get paired with their corresponding IR  $T_B$ , which is often larger (warmer) than other localized pixels that were correctly identified as rainfall. The end result can at times be a very light rainfall (under  $0.5 \text{ mm h}^{-1}$ ) that incorrectly gets assigned to regions in subsequent IR imagery, until these falsely-identified PMW points are discarded from the suspect 2-degree histogram box (usually after the next LEO overpass). The opposite effect also occurs, when the PMW algorithm rain/no-rain screen fails to identify regions of light rain. That is, these no-rain pixels get paired with a smaller (colder) IR  $T_B$  compared to other localized pixels. The result is that the zero-rain IR temperature threshold gets assigned too small of a value and the lookup table assigns zero or a very small value to subsequent IR imagery. While we cannot say for certain that misses and false alarms by the PMW screening algorithm are the cause of this, one can state that

owing to its very nature, any caveats of the PMW instantaneous rain algorithms eventually manifest themselves in the blended technique results. The amount of time that these (or other) PMW data are retained in the blend is determined by the tuning parameters described in Section 2 (box size, percent coverage,  $\Delta t$  and  $\Delta d$ ).

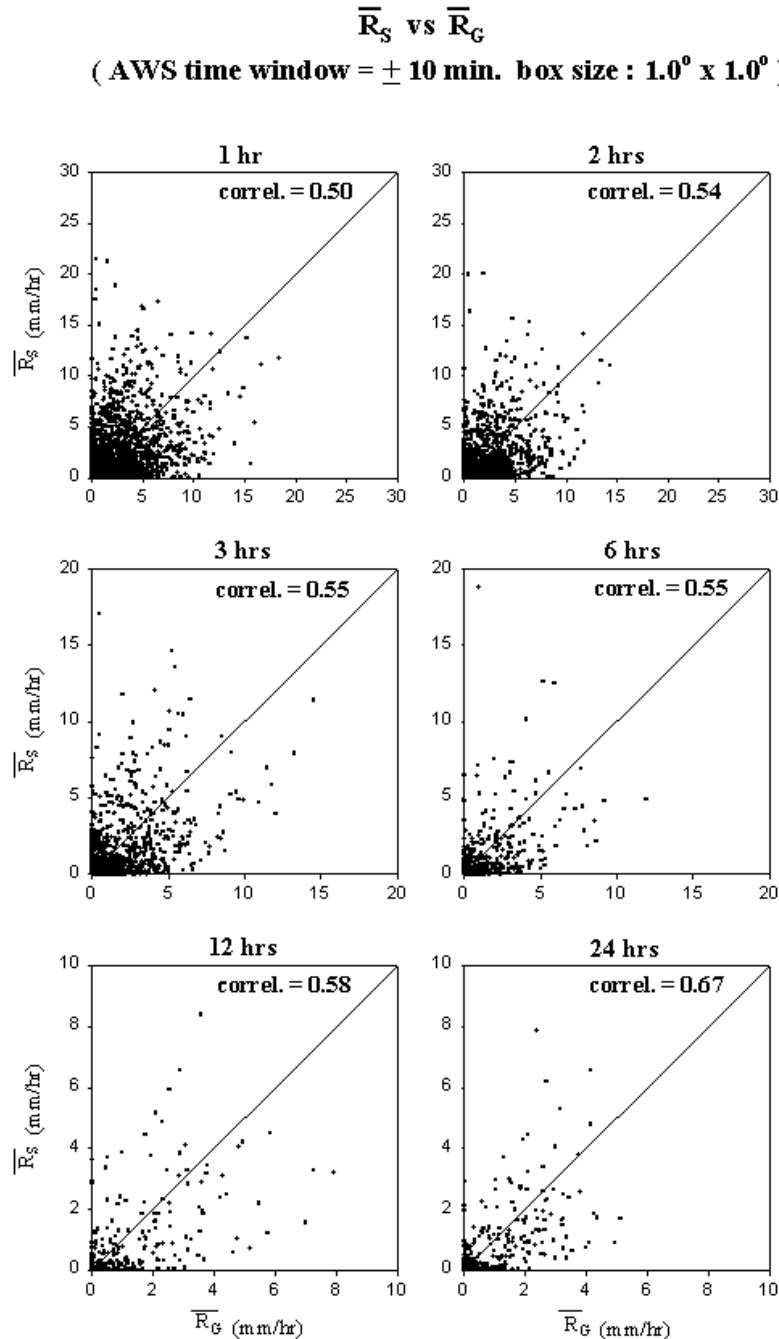


Figure 5. Scatter plots of the observed KMA AWS rain gauge ( $R_G$ ) and blended satellite technique-derived ( $R_S$ ) average rate rates at a fixed 1-degree resolution spatial average over Korea. From upper left, the six panels are for time averages of the AWS data over 1-hour, 2-hour, 3-hour, 6-hour, 12-hour, and 24-hour time intervals. A  $\pm 10$  minute window was used to average the AWS gauge data, centered about the time of the GMS satellite observation of Korea.

Fig. 6a and 6b depict the results from the analysis at this and other space and time scales in a two-dimensional format, where the spatial average and averaging period determine the abscissa and ordinate, respectively. The correlation, mean bias and root-mean-square error (RMSE) are each contoured for AWS time windows (gauge averaging time centered about the GMS observation time) of  $\pm 1$  (Fig. 6a) and  $\pm 10$  minutes (Fig. 6b) (other time windows are not illustrated here). The different time windows produce different results, owing to the variable fallout times of the hydrometeors from within the cloud, and the increased number of gauges in the average as the window is widened. However, there appears to be a sharp improvement when the time window is widened to  $\pm 10$  minutes, which a typical hydrometeor fallout time in tropical clouds (Soman et al., 1995) and from this point on the  $\pm 10$  minute AWS-GMS time window is assumed.

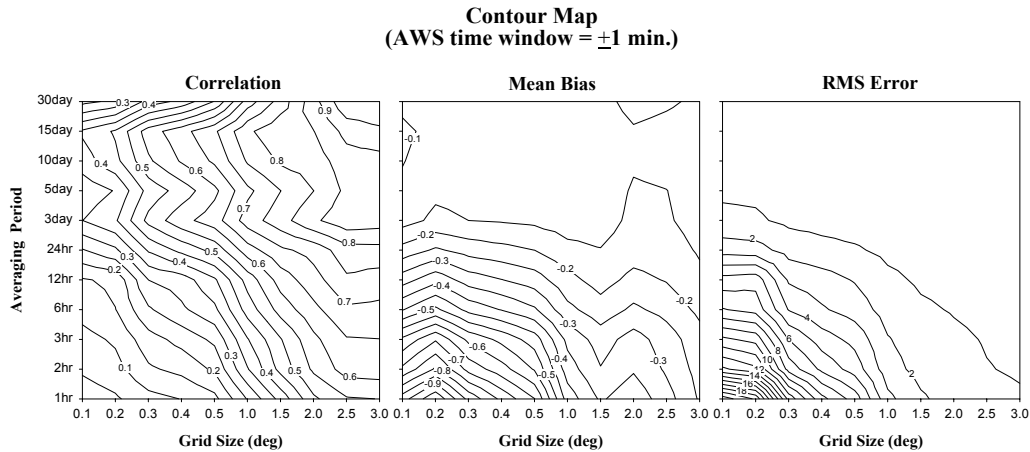


Figure 6a. Space-time contour plots of the correlation coefficient, root mean square error and mean bias for an AWS time window average of  $\pm 1$  minutes. The time window is centered about the time of the GMS satellite observation of Korea. The abscissa and ordinate of each contour plot denotes the spatial and temporal scales, respectively, used to average the gauge data and the blended satellite technique estimated rain.

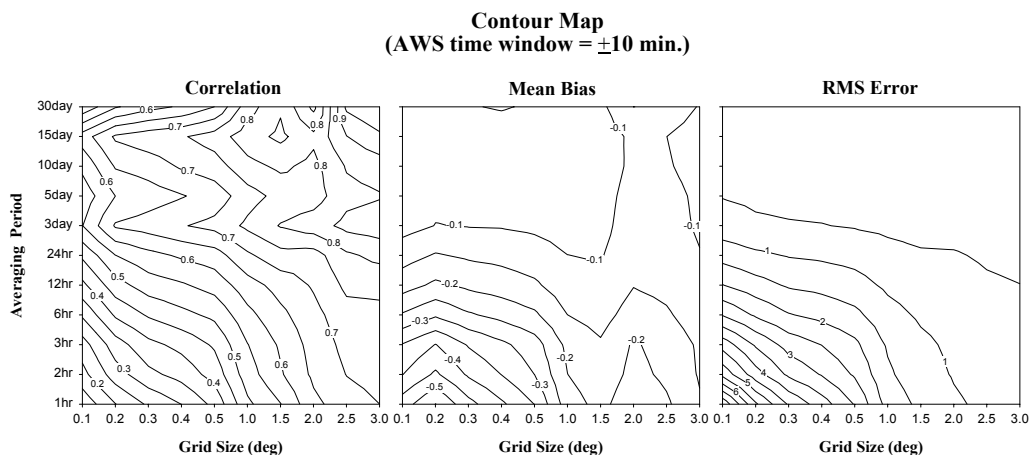


Figure 6b. Same as Figure 6a, but the AWS time window average is expanded to  $\pm 10$  minutes.

As expected, all three parameters improve as either the averaging period is increased or the grid size is coarsened. The contours do not flow smoothly at the longest time intervals due to the resultant small number of data points available from the finite 3-month period. Likewise, the small size of the Korean Peninsula produces a small number of data points when the data are averaged

over the coarsest space scales. The blended technique is biased slightly negative (-0.1, or 10% low) once the time interval exceeds 3 days, falling to about -0.35 (35% low) at 3-hour/0.25-degree scales. One possible explanation for the bias behavior is that as the time scale is shortened, extreme heavy precipitation events are less likely to be captured by a LEO overpass. Since the nature of the blended technique is to retain some of the most recent rainfall history (a residual “memory effect”), there is a gradually increasing (rather than sudden) negative bias. The RMSE is about  $0.5 \text{ mm h}^{-1}$  for time intervals exceeding 3 days, and degrades to near  $3.5 \text{ mm h}^{-1}$  at 3-hour/0.25-degree scales. The correlation coefficient can be as high as 0.8 for 12-hour averages, but only when the grid size exceeds 2.5 degrees. Most notably, the correlation begins to fall off quickly once the time average drops below one day, and/or the spatial scale falls under 1-degree, and this same sort of behavior is evident in the RMSE, and less so in the mean bias. This could be because the RMSE is more affected by the relatively few large precipitation events, whereas the correlation is affected by the large number of zero or near-zero rain rate points. As the time and/or space scale shrink, there are fewer heavy rain events, and the large number of zero or small rain rates, which show a large scatter, dominates the correlation coefficient.

Inherent in the inner workings of this type of blended technique is a residual “memory effect” whereby a certain amount of previous-time PMW information is retained in the statistical blend, and provided to subsequent geostationary update cycles. The effect is dependent upon the LEO revisit time, which at the latitude of Korea is about 12-hours (worst case) for the 4-satellite (3 SSM/I and the TMI) constellation. As mentioned, the current 2-degree box size for the statistical matching represents a tradeoff between the overall revisit from the intermittently-spaced LEO satellite constellation (longer revisit requires a larger box size) and the need to capture “localized” rainfall characteristics and still have a sufficiently large number data points to perform a statistical histogram matching (small scale rainfall requires a smaller box size). The rapid decay of the correlation and RMSE statistics below the daily time scale may be reflecting the fact that below this scale, the blended technique estimates are often tuned with rainfall information from a somewhat earlier stage (several hours earlier) in the localized rainfall evolution, and don’t always correlate well with the current rainfall evolutionary state. At time scales greater than one day, the correlation remains quite high even at the finest spatial scales, suggesting that this type of memory effect may average away past a certain time scale. While this is a plausible explanation, there are certainly other factors at work, most notably the nature of sporadic and intermittent rain evolving over a limited number of gauges. By analyzing the three month period, there are many short time-scale periods that are averaged together, some with intermittent, sporadic rainfall and others with more widespread rainfall, therefore the gauge-satellite effect should be averaged to some undetermined extent. Even so, we can state that below some minimum combination of space and time scales, there is most likely dependence between the overall LEO constellation revisit and the performance of this type of blended technique.

For NWP rainfall data assimilation requirements, the rainfall estimation error should be specified as a function of the average rain rate over the estimated space-time interval (e.g. percentage error at 1, 5, 10  $\text{mm h}^{-1}$ , etc). NWP variational assimilation techniques typically are based upon a minimization function, which requires knowledge of both the forecast and the observation (rainfall analysis) errors. If the forecast error is large, then the observed rainfall analysis will be increasingly allowed to contribute to the model initialization, and vice versa. The 3-hour/0.25-degree RMSE of  $3.5 \text{ mm h}^{-1}$  was computed for all rain rates, and this would translate to a 35% error at  $10 \text{ mm h}^{-1}$ .

The KMA gauge analysis provided validation over the three month summer interval, which are indicative of summer monsoon wet conditions, and were done during a time when the AMSU-B sensors had not yet been added to the LEO constellation used in the blended technique. To examine the overall characteristics and performance of the technique, a longer validation time interval is needed, preferably one that covers both tropical and mid-latitude rainfall regimes and summer and winter seasons. In the following section, we present validation statistics over the Australian continent from one calendar year, during which time two of the AMSU-B satellites were

incorporated into the blended technique. In doing so, our intent is not to develop nor validate a climatological rainfall technique, but rather to use the validation results from daily and monthly time scales to examine characteristics and areas where the blended technique has strengths and other areas where it needs improvement.

#### 4. Validation with the Australian continental analysis

The Australian Bureau of Meteorology (BOM) maintains a national rain gauge network consisting of over 6000 sites that measure 24-hour accumulated rainfall at approximately 9 AM local time. On average, 2000 of these stations report daily rainfall in near real time to the BOM rainfall analysis system. The objective analysis scheme is based upon a multi-pass inverse-distance weighting scheme to map the rainfall data onto a 0.25-degree grid over the Australian continent and Tasmania (Weymouth et al, 1999). Fig. 7 displays the density of the gauges, which ranges from more than 50 per 1-degree grid box in the populated southeast to no gauges at all in some interior regions.

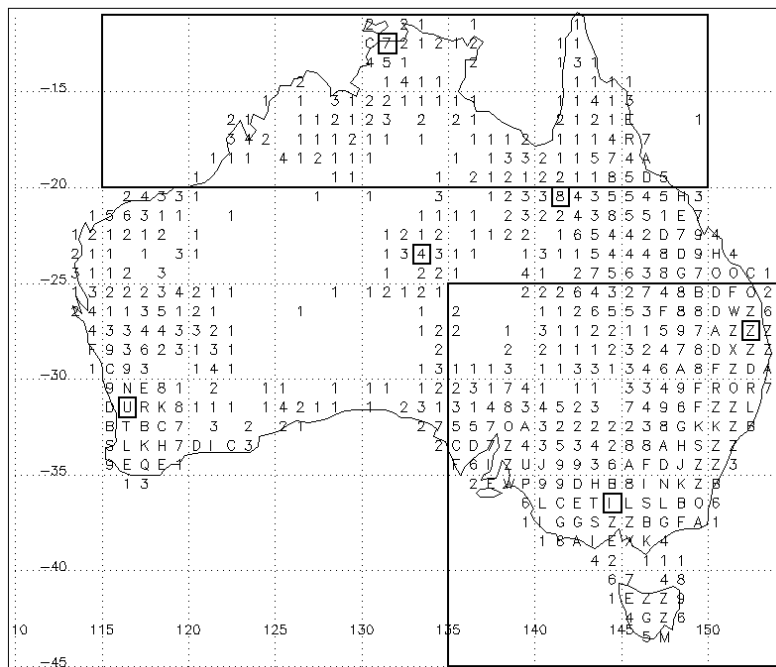


Figure 7. Density of rain gauges within 1-degree boxes comprising the continental rain gauge network operated by the Australian Bureau of Meteorology (BOM). The numbers correspond to 1, 2, 3, etc. gauges per box, while the letters correspond to A=10, B=11, C=12...Z=35+ gauges/box.

The purpose of this section is to examine the characteristics of the blended technique at daily and monthly time scales over both winter and summer seasons, tropical and mid-latitude rainfall regimes, and regions of orographic uplift (e.g. western Tasmania, where the average annual rainfall exceeds 3 m). The unique yearly climatology throughout the Australian continent makes this possible. This was carried out for twelve months beginning in April 2001, during a time when the AMSU-B data from NOAA-15/16 (NOAA-17 became available in mid-2002) were added to the LEO constellation used to drive the blended technique. For comparison, the blended technique performance is also compared against that of a simple merge of all 6 (3 SSM/I, TMI, and 2 AMSU-B) satellite-derived instantaneous rainrates (averaged over one day and one month). We also will perform a test of the sensitivity of the blended technique to situations where one or more satellites are omitted from the LEO constellation used to drive the blending procedure.

After each day's 0 UTC 24-hour daily precipitation accumulations from the blended technique were completed, these blended technique datasets as well as the associated merged SSM/I+TMI+AMSUB datasets were transferred to the BOM for an automated comparison with the rainfall analysis system. The blended technique rainfall datasets were reduced from their 0.1-degree processed resolution to the 0.25-degree resolution of the rainfall analysis system. The top two panels of Figure 8 are daily time series plots of the observed rain rate ("OBS", solid line), the blended technique estimate ("GEO", long dash), and the merged estimate ("SSM/I+TMI+AMSUB", short dash), where the satellite-derived averages were formed with points at all rainfall-reporting stations. A 25S latitude was used to separate tropical and mid-latitude rainfall regimes. To better depict the day-to-day fluctuations, we have only plotted data from three months beginning in January 2002. This summer period corresponds to the wet season in the tropical Northern Territories (averaging near 400 mm in January in Darwin) and the driest period in Western Australia (averaging about 10 mm in January in Perth).

The bottom two panels of Fig. 8 depict the associated rain area results. In the tropical regime, both satellite estimates were biased low, in accord with the Korean Peninsula verification in Section 3. The blended technique was the best performer, especially for the heaviest rain events in mid-January and February. In the drier mid-latitude regime, the blended technique tracked the observed values better, but with no clear bias one way or the other. For the dry days in late March, neither estimate had very good performance. Similar characteristics were noted in the rain area results. Overall, for this period the blended technique performed best in the tropical regime and for the heaviest rain days in both regimes. In the mid-latitudes, the blended technique appeared to do well for the heavy rain days, with no clear winner in the light rain days. Overall, the rain area was underestimated by all satellite techniques. The blended technique was biased high in several instances, which we will further comment on below.

Fig. 9a-9f depict the daily correlation, RMSE and mean difference over this same time period, for both tropical and mid-latitude regimes. We first verify consistency with the results from the KMA raingauge analysis of the previous section at the 24-hour and 0.25-degree time and space scale combination. From Figure 6b, at these scales the correlation and RMSE are approximately 0.55 and  $1 \text{ mm h}^{-1}$ , respectively. In comparison, the BOM analysis shows a wide fluctuation in these same daily values, depending upon the number of reporting gauges and the average observed rain rate, but for the heavy tropical rain (as a first approximation an analogy to the summer monsoon season in Korea) the values are in fairly good agreement (RMSE is in units of  $\text{mm d}^{-1}$ ). The mean difference is deceiving unless one looks at the average observed rain alongside it. For example, the blended technique exhibits near zero mean difference in the tropics in March (an unusually dry month), but several extreme positive and negative spikes in the wetter January and February, respectively. In the mid-latitudes, the situation is similar, but less extreme.

As noted in the South Korea analysis, the performance of this type of blended technique is time sensitive, determined to a some extent by the accuracy of the instantaneous PMW retrieved rainrate itself, and the age of the most recent LEO overpass. Over the latitude range of Australia, the worst-case revisit of the six-satellite LEO constellation is quite good (between 5-6 hours), and 2-3 hours on average. The Version-5 of the GPROF algorithm used in the TMI 2A12 over-land rainrate algorithm draws upon a cloud-radiation database that is dominated in number (thousands) by over-ocean cloud profiles, and a much small number (less than 50) of over-land cloud profiles. Consequently, the over-land TMI-derived rainrate histogram will show "spikes" when the retrieval algorithm hits upon the same profile repeatedly. Although it is difficult to tie together cause and effect when trying to tie this or related behavior to the observed trends in the blended technique's mean bias, the most likely explanation may have to do with both the amount and frequency of extreme heavy rain events that are captured by the LEO constellation overpasses, and the quality of the PMW estimate itself.

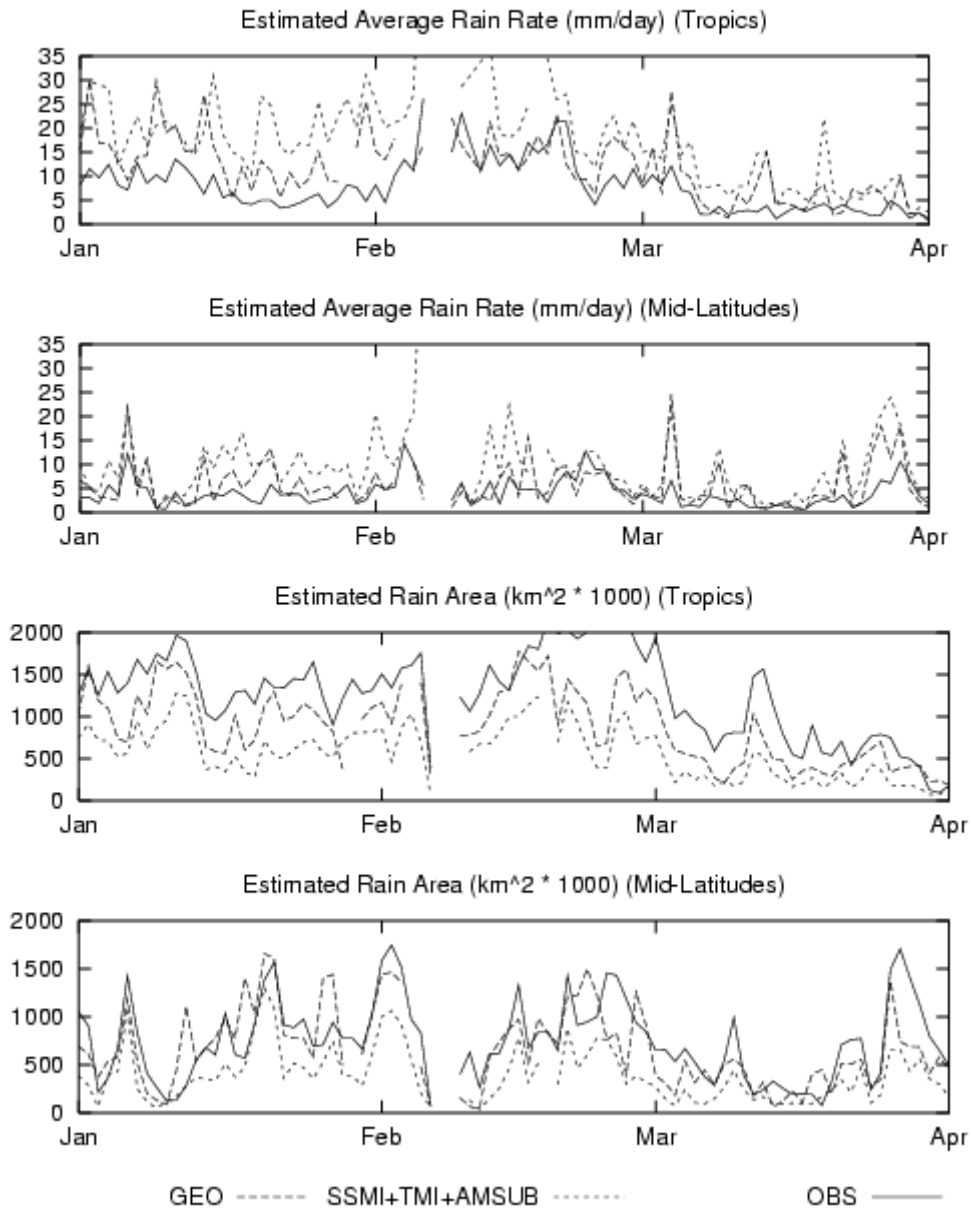


Figure 8. (A) Estimated daily average rain rate from the blended technique (GEO), and merged SSM/I+TMI+AMSU-B estimates plotted against the Australian rainfall analysis system (OBS) from 1 January to 1 April 2002, over the tropical regime (north of 25S latitude). (B) Same as (A) but for mid-latitudes (south of 25S latitude). (C) Same as (A) except the daily rain area is plotted for the tropical regime. (D) Same as (C) except the mid-latitude region is plotted.

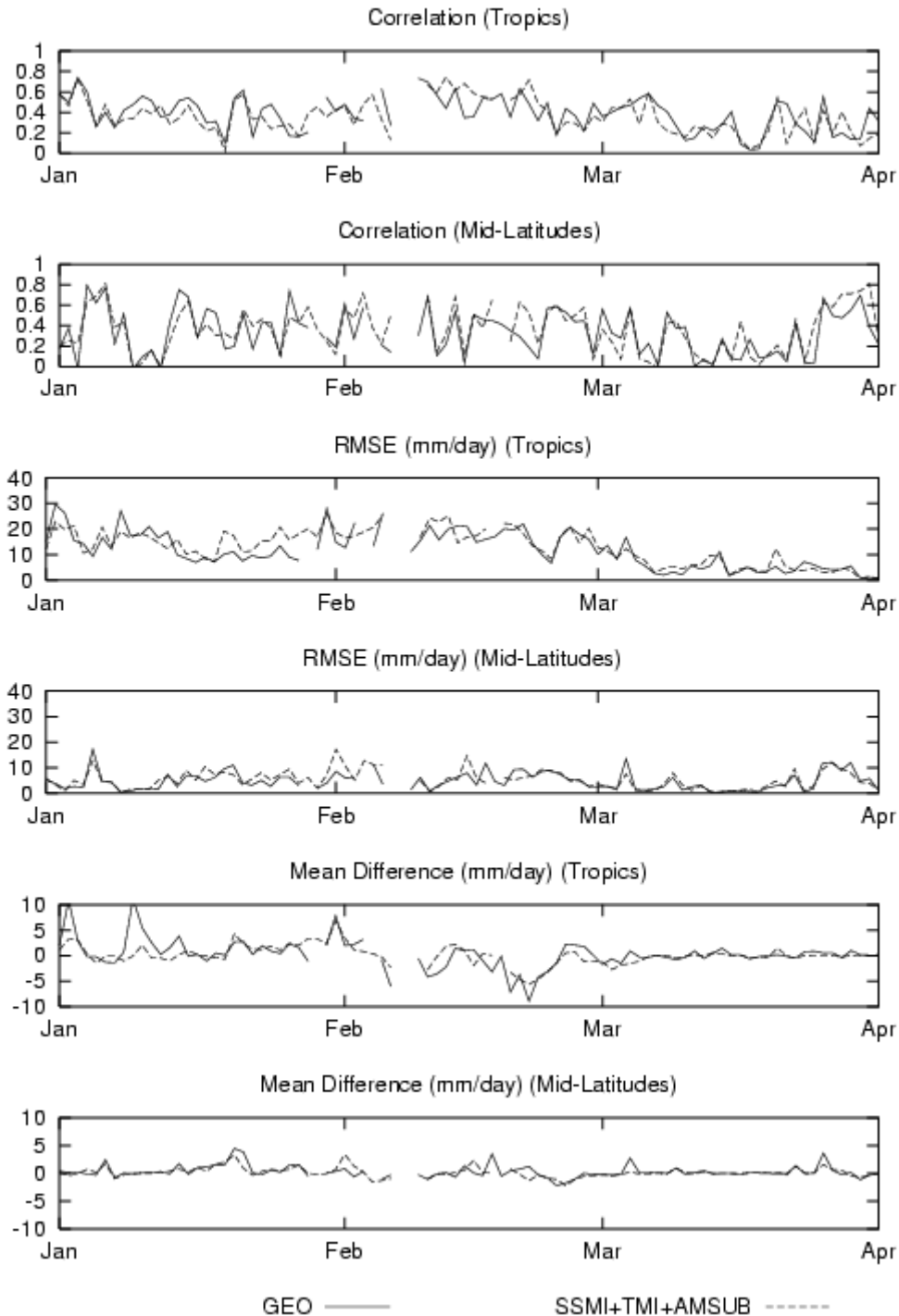


Figure 9. (A) Daily correlation coefficient of the blended technique (GEO), and merged SSM/I+TMI+AMSU-B estimates versus the observed values from the Australian rainfall analysis system, from 1 January to 1 April, 2002 over the tropical regime north of 25S latitude. (B) Same as (A) except for the mid-latitude region is plotted. (C) and (D) are the same as (A) and (B), except that the daily root mean square error (RMSE) is plotted. (E) and (F) are the same as (A) and (B) except that the daily mean difference is plotted.

Next, the comparison between the Australian rain gauge analysis system and the blended technique is performed at the monthly time scale. The purpose of this is not to examine the capability of the blended technique as a monthly scale, climatological estimator of global precipitation (there are other more thoroughly examined techniques specifically for this purpose), but to average away the day-to-day fluctuations in the statistics shown in Fig. 8 and 9, and

examine any persistent trends blended technique as manifested in the skill scores or validation statistics. To ease comparison, Fig. 10 and 11 are identical to Fig. 8 and 9, except that the abscissa now contains only 15 points, each representing the overall monthly value between 1 April 2001 and 1 July 2002, and we show three estimates, the blended technique (“GEO”), the merged 6-satellite (“SSM/I+TMI+AMSUB”), and the merged 3-satellite SSM/I-only (“SSM/I”).

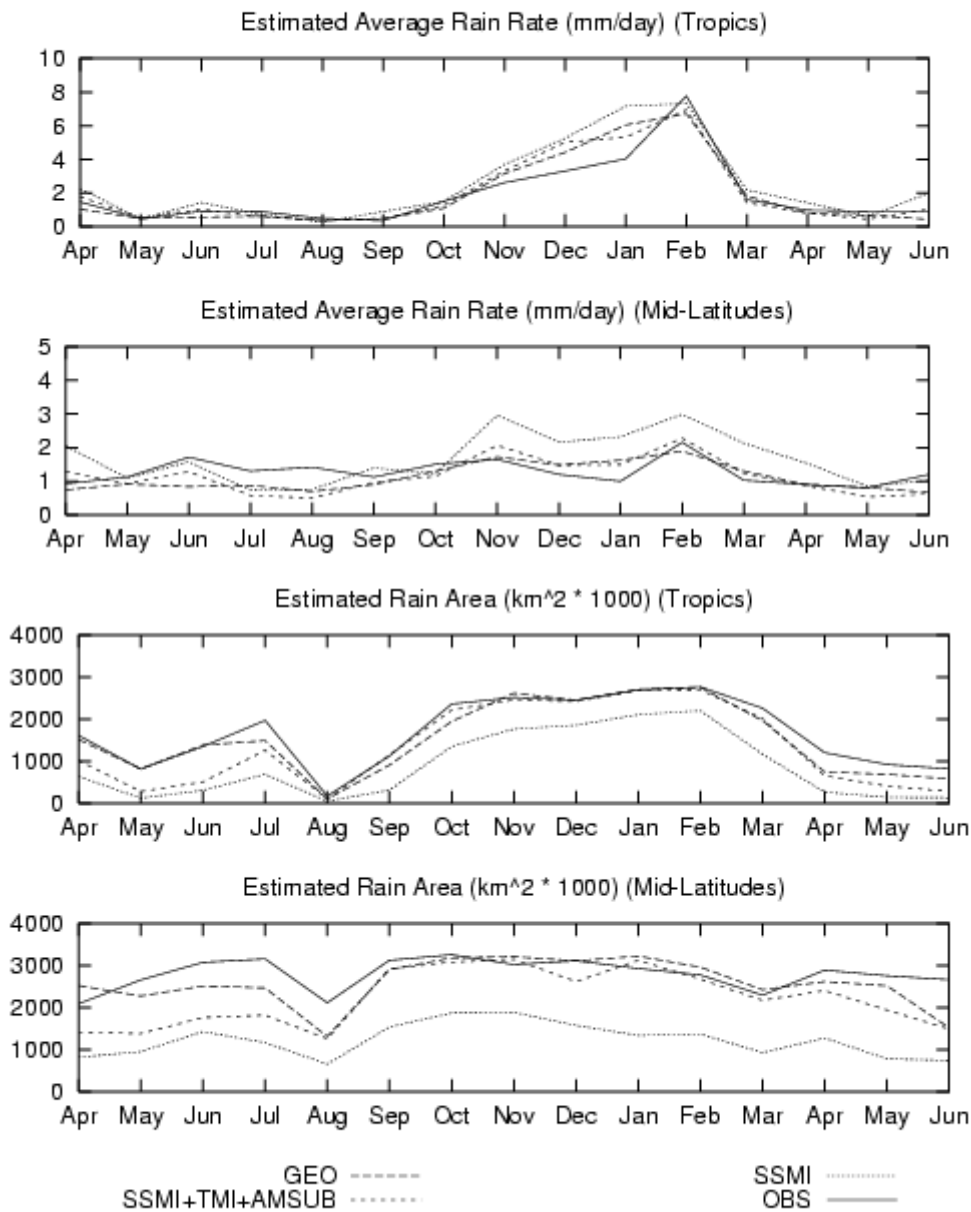


Figure 10. Same as Fig. 8, except that the monthly average values from 1 April 2001 to 1 July 2002 are plotted, as well as the merged SSM/I-only estimates

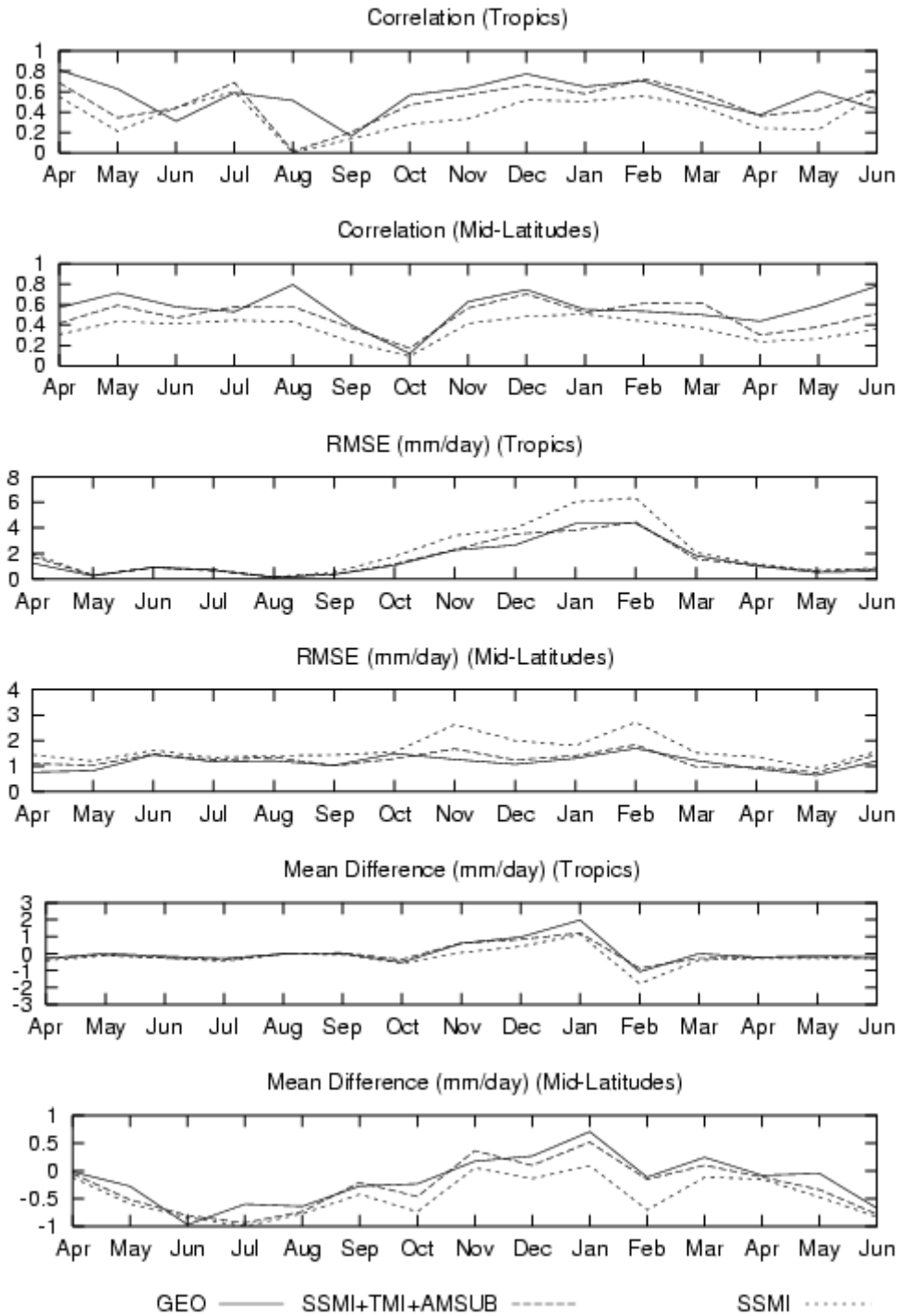


Figure 11. Same as Fig. 9, except that the monthly average values from 1 April 2001 to 1 July 2002 are plotted, as well as the merged SSM/I-only estimates.

From Fig. 10, both the blended technique and the SSM/I+TMI+AMSUB both display similar values of continental-averaged rainrate over the entire 15-month period. The bias is near zero for all cases except during the wettest months where all techniques are biased high. In the mid-latitudes, neither technique performed especially well, but it is clear that the addition of the AMSU-B and TMI data greatly improve the statistics of a simple satellite merged technique (comparing SSM/I and SSM/I+TMI+AMSUB performance). The estimated rain area is well captured by either the blended technique or the SSM/I+TMI+AMSUB in the tropics. In the mid-latitudes, the rain area is

underestimated in the dry summer months by all techniques, but the blended technique has the best performance of all three.

In Fig. 11, the monthly statistics clearly depict the behavior of the blended technique. The performance falls off in the driest winter months June-September for both tropical and mid-latitude regimes as indicated by the correlation. In the tropics, the RMSE increases during the summer months as rainfall amounts increase. In the wettest tropical month of February, the mean difference becomes slightly negative, which concurs with the KMA raingauge analysis trends noted in the previous section. The performance of the blended technique clearly falls off in the mid-latitude regime, where IR-based rainfall techniques are known to have their greatest shortcoming (Ebert and Manton, 1998).

## 5. Impact of the AMSU-B rainfall observations

In the previous section, it was shown that by simply adding the AMSU-B and TMI rainrate estimates to a simple merged-sensor technique improved the overall monthly validation statistics, presumably due to the more frequent time sampling of the diurnal precipitation process captured by the TMI orbit and the morning and afternoon NOAA-15 and NOAA-16 orbits. However, in order to determine the impact of adding the non-rain radiometers such as the AMSU-B into the blended technique, we have to investigate the monthly performance of various parallel versions of the blended technique, where each version employs a different underlying LEO constellation. Specifically, the March 2002 observed validation data were compared against four versions of the blended technique, each employing LEO constellations denoted by A (TMI only), C (3 SSM/I only), D (3 SSM/I+TMI) and E (3 SSM/I+TMI+2 AMSUB). Table 1 summarizes the March 2002 analysis validation results. Initially, we expected the performance of the blended technique version using the (six satellite) LEO constellation E to be superior to the version using the (four satellite) constellation D, since the NOAA-16 satellite (with an AMSU-B) partially fills the early afternoon local time sampling gap. However, during this month, there was no clear winner, the four-satellite version even slightly outperformed the six-satellite version in average rain rate and correlation. Similar inconclusive results were noted during April and May 2002.

Constellation Used in Blend	Avg Rain	Rain Area	RMSE	Mean Diff	CC	HSS	Bias Score	POD	FAR
A (1 sat)	2.18	2114	2.08	0.35	0.59	0.35	0.94	0.83	0.11
C (3 sats)	1.02	1263	1.49	-0.84	0.67	0.27	0.56	0.54	0.03
D (4 sats)	1.77	1875	1.51	-0.11	0.63	0.37	0.83	0.76	0.08
E (6 sats)	1.84	1965	1.82	-0.01	0.51	0.31	0.87	0.77	0.11
<b>Observed</b>	1.60	2261							

Table 1. Overall March 2002 statistics for the tropical (above 25S latitude) Australian rainfall validation, as a function of the constellation configuration used to update the blended technique. CC= correlation coefficient, RMSE= root mean square error, HSS= Heidke skill score, POD= probability of detection, FAR= false alarm ratio. Average rain, RMSE, and mean difference units are  $\text{mm day}^{-1}$ , and rain area is given in units of ( $\text{km}^2 \times 1000$ ).

In an attempt to explain this finding, we took advantage of the fact that the inclined tropical orbit of the TRMM satellite positions the along-track tracks so as to enable frequent time- and space-intersections with the sun-synchronous, near-polar orbits of the DMSP and NOAA satellites, and therefore TRMM could be used as a “reference” to examine if there was any systematic bias

between the SSM/I and AMSU-B rainrate estimates (relative to the TMI 2A12 estimates). All orbits of data between November 2001 and January 2002 were processed, and very-fine time and space coincident TMI-SSM/I and TMI-AMSUB pixel pairs were extracted using a maximum allowed time and space offset of 1-minute and 10-km, respectively. These data were further separated into over-ocean and over-land pixels (coastal pixels were discarded), and no-rain and rain pixels depending upon the TMI 2A12 algorithm rain flag. In order to account somewhat for varying spatial resolution of the different instruments, the TMI data were averaged over a 3x3 box in the SSM/I case, and between a 3x3 and a 5x5 box in the case of the AMSU-B, depending upon the AMSU-B across-track scan position. The two left-hand panels of Fig. 12a depict (for the rain flagged pixels only) the scatter plot of the over-ocean SSM/I vs. TMI, and over-ocean AMSUB vs. TMI. Fig. 12b is the same plot, for the over-land pixels. The wide scatter in the data is evidence of, among other things, variations in the instantaneous PMW rainfall algorithms even when they are pointing to the same on-Earth location, instrument beamwidth differences, and from differences arising from different azimuthal viewing directions of the same cloud.

In order to eliminate some of the scatter, these middle column depicts the case where the pixel collocation time is expanded to 15 minutes and the spatial offset was maintained at 10-km, after which the coincident data are further bin-averaged to 1-degree (the larger collocation time allows more pixels, and the bin-averaging removes some of the azimuthal viewing angle differences). The right hand column depicts the same situation for a 1-hour collocation offset and a bin averaging of 2.5-degrees. In the last two columns, a positive bias of the over-ocean AMSU-B rainrate relative to TMI becomes evident, and a slight negative bias of the over-ocean SSM/I rainrate relative to the TMI for rainrates  $< 2 \text{ mm h}^{-1}$ .

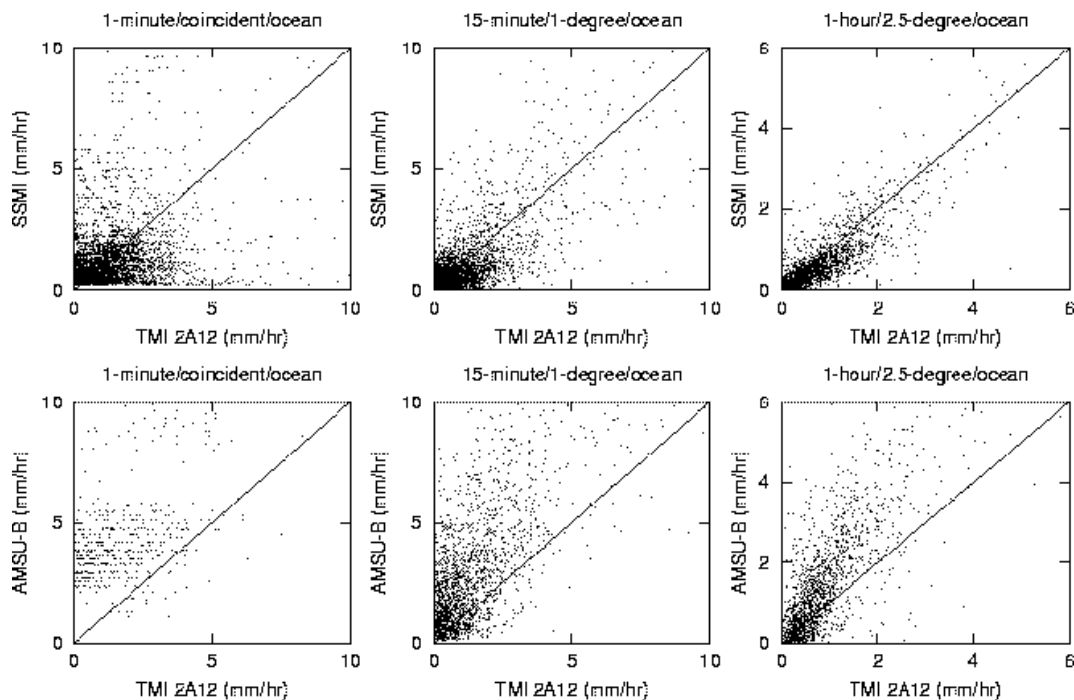


Figure 12a. Scatter plots of the SSM/I-derived rainrate and the AMSU-B-derived rainrate vs. the TMI 2A12-derived rainrate for all pixels when the TRMM orbit intersected the DMSP and NOAA orbits, for three months between November 2001 and February 2002. All instantaneous SSM/I-TMI and AMSUB-TMI pixel pairs are initially collocated to within 10-km in space, and further within 1-minute, 15-minutes, and 1-hour in observation time. The data are then further binned into 1-degree and 2.5-degree boxes. First row: SSM/I vs. TMI rainrates for a 1-minute offset and no additional spatial averaging, 15-minutes offset and 1-degree spatial averaging, and 1-hour offset and 2.5-degree spatial averaging. All pixels are for over-ocean. Second row: Same as first row but with AMSU-B replacing the SSM/I.

•

In the over-land situations, the same bin averaging reduced less of the scatter between the PMW algorithms, and it is difficult to identify any significant biases, although the variance between the TMI, AMSUB, and SSM/I PMW algorithms is much larger. The over-land PMW algorithms these sensors are largely influenced by the 85 GHz scattering-based channels (89 GHz for the AMSU-B), where the variability in ice optical thickness for a given underlying rainfall rate gives rise to a wider variability in the 37 and 85 GHz  $T_B$  (Vivekanandan et al., 1991). In Section 2, we explained that the blended PMW-IR procedure uses a maximum time offset  $\Delta t=15$  minutes and maximum spatial offset  $\Delta d=10$  km in the PMW-IR coincident data alignment procedure, and a box size of 2-degrees for the individual histograms. For each 0.1-degree IR pixel, the closest 2-degree box and the eight surrounding boxes are located, and an inverse-distance weighted average is computed from the nine lookup table-derived rainrates in order to minimize rainrate discontinuities across box boundaries. Therefore, the rainrate estimates produced by the blended technique for land pixels within approximately 4-degrees latitude or longitude of the Australian coastline will be affected by both the over-land and over-ocean PMW inter-sensor bias effects (the inverse-distance weighting reduces the effect as one moves farther from a coastline). Far enough inland, only the over-land PMW inter-sensor bias affects affect the land pixels. But since a large percentage of the tropical and mid-latitude Australian continental rain falls within 4-degrees latitude or longitude of a coast, the addition of the AMSU-B data to the blend therefore adjusts the blended technique with a larger rainrate (relative to TMI) than if an SSM/I overpass had occurred at the same time. Referring to the 15-minute/1-degree bias plots in Fig. 12a (closest to the above-mentioned scales of the blended PMW-IR procedure), this might explain the slightly larger average rain and rain area noted in Table 1 for the constellation E (with the AMSU-B instruments) than for the constellation D case (without the AMSU-B sensors). However, there could be other factors at work and so we can only postulate this. One way to account for the presence of inter-sensor biases in the blended technique is to declare that the TMI rainrates will be the PMW rainrate “reference”, and to adjust the SSM/I and AMSU-B rainrates accordingly, so that the rainrates derived from each member of the underlying LEO constellation are consistent.

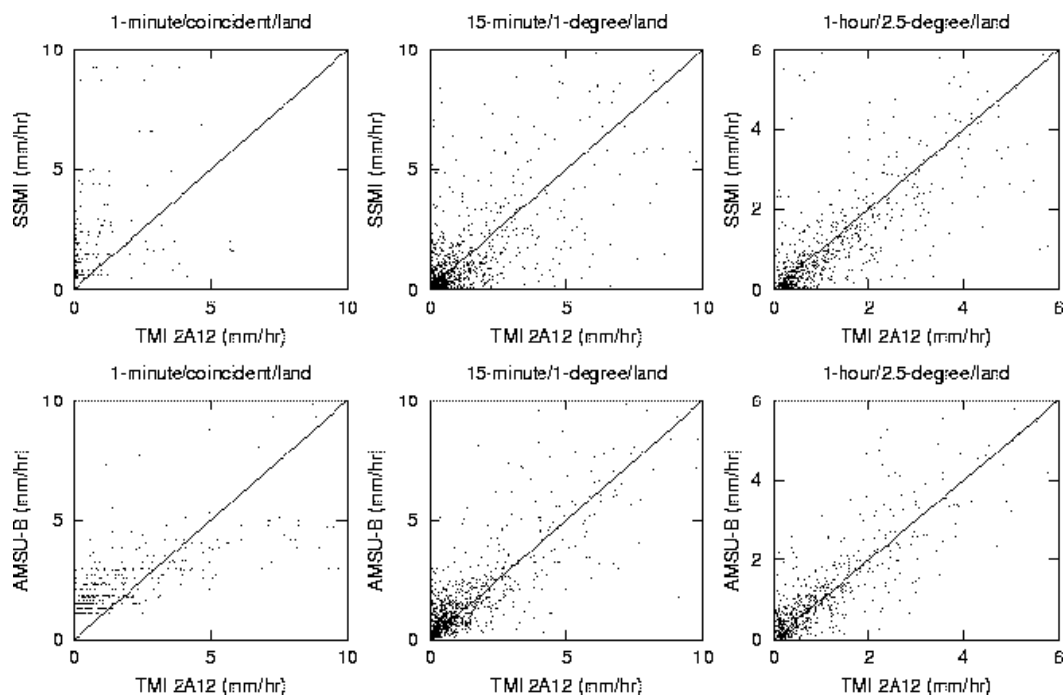


Figure 12b. Same as Fig. 12a, except for over-land pixels only.

Lastly, we note that the above information gathered by the space and time-intersecting LEO satellite overpass analysis is very similar to the situation faced by the proposed Global Precipitation Measurement (GPM) mission. It is envisioned that GPM will include various blended and merged precipitation estimates at telescoping space/time scales (e.g., 0.1-degree/3-hour up to 5-degree/1-month), produced by a LEO constellation containing different types of PMW sensors and their various instantaneous rainrate algorithms. To do so require a reference satellite (the GPM core) and a means to transfer the information gathered from intersection of the GPM core with the other constellation members. The transfer should be done across various space-time boundaries so as to best produce a final global rainfall rate product consistent between all constellation members.

## 6. Conclusions

We have presented a series of over-land validation statistics from comparisons between satellite-derived rainfall estimates from a blended IR-PMW precipitation technique and ground-based rainfall observations gathered from operationally-maintained raingauge networks in Korea and the Australian continent. The bias, RMS error, and correlation coefficient were computed at various space and time scale combinations owing to the gauge density and the 1-minute sampling capabilities of the Korean AWS network. While precise gauge-satellite comparisons are by nature not truly possible, the gauge density and the 1-minute sampling capabilities of the Korean AWS network does reduce (but not eliminate) fundamental spatial and temporal offsets between observations and estimates, and provides a basis for gathering error statistics at sub-daily time scales and sub-one-degree spatial scales. Finer than approximately 1-day and one-degree time and space scales, respectively, a rapid decay of the error statistics was obtained by trading off either spatial or time resolution. Beyond a daily time scale, the blended estimates were unbiased and with an RMS error of no worse than  $1 \text{ mm d}^{-1}$ . Analysis of one years (April 2001-April 2002) worth of daily comparisons (24-hour totals) between the BOM continental Australian raingauge analysis system and the blended technique demonstrated the performance of the blended technique at both tropical and mid-latitude regimes, summer and winter seasons, and surface regions ranging from desert to steep terrain responsible for orographically enhanced precipitation. The blended technique performed very well in the tropical regime above 25S latitude and for the heavy rainfall; over the mid-latitudes, the performance suffered for both summer and winter seasons and regions of steep terrain.

A blended IR-PMW satellite-based precipitation technique is (by the nature of the ever-expanding suite of LEO PMW sensors and multispectral geostationary imagers) a constantly evolving type of technique. As described in this article, its current implementation is admittedly crude in several respects, namely the use of a single common  $11\text{-}\mu\text{m}$  IR thermal channel, and no separation of stratiform and convective rain situations. Next-generation geostationary imagers such as SEVIRI (Schmetz et al., 2002) are becoming increasingly sophisticated and their expanded spectral and time-update capabilities have yet to be fully exploited for cloud microphysical and phase information. In the current blending technique described in Section 2, a statistical histogram matching procedure is used to tie together the PMW and IR observations from LEO and geostationary sensors. Originally, this type of technique was developed for radar rainfall applications over a sufficiently wide area and a time interval sufficient to capture many individual rain events. Its utility when it is extrapolated down to the short time/space scales attempted here has yet to be fully examined, and other means to blend the information together need be examined and tested.

The proposed international Global Precipitation Mission (GPM) is a constellation mission consisting of a primary, non-sun-synchronous orbiting reference satellite with a PMW radiometer (GMI) and dual-frequency radar (DPR), and a constellation of various LEO satellites from U.S. government and international agencies (Fleming, 2002). One objective of GPM is to provide enough sampling to reduce the uncertainty in short-term rainfall accumulations. Moreover, the ground validation

phase of GPM is being designed to include a means to produce bias and uncertainty factors that are a function of space, time and rainrate, as well as local-domain space-time rain error covariance structures as a function of space and time (Bidwell et al., 2002). For many applications, the rainfall products to be produced by the GPM constellation may be sufficient by themselves, but other applications may still require blended satellite techniques to provide data over regions of the Earth that are left uncovered by the GPM constellation orbit pattern.

*Acknowledgments* - The first author gratefully acknowledge the support of his research sponsors, the Office of Naval Research, Program Element (PE-060243N) and the Oceanographer of the Navy through the program office at the Space and Naval Warfare Systems Command, PMW-155 (PE-0603207N).

## 7. References

- Adamo, C., R. Solomon, S. Dietrich, and A. Mugnai, 2002: Rainfall monitoring at the geostationary scale: Potential of lightning data in a rapid update approach. *Proc. 3<sup>rd</sup> EGS Plinius Conf. on Mediterranean Storms*, R. Deidda, A. Mugnai, and F. Siccardi, Eds., GNDCI, Publ. N. 2560, 123-128.
- Adler, R. F., A. J. Negri, P. R. Keehn, and I. A. Hakkarinen, 1993: Estimation of monthly rainfall over Japan and surrounding waters from a combination of low-orbit microwave and geosynchronous IR data. *J. Appl. Meteor.*, **32**, 335-356.
- , G. J. Huffman, D. T. Bolvin, S. Curtis, and E. J. Nelkin, 2000: Tropical rainfall distributions determined using TRMM combined with other satellite and rain gauge information. *J. Appl. Meteor.*, **39**, 2007-2023.
- Ba, M., and A. Gruber, 2001: The GOES Multispectral Rainfall Algorithm (GMSRA). *J. Appl. Meteor.*, **40**, 1500-1514.
- Bauer, P., D. Burose, and J. Schulz, 2000: Rain detection over land surfaces using passive microwave satellite data. *ECMWF Tech. Memo. No. 330*, ECMWF, Reading, England.
- , J. F. Mahfouf, W. S. Olson, F. S. Marzano, S. di Michele, A. Tassa, and A. Mugnai, 2002: Error analysis of TMI rainfall estimates over ocean for variational data assimilation. *Q. J. Roy. Meteor. Soc.*, **128**, 2129-2144.
- Bidwell, S. W., S. Yuter, W. J. Adams, D. F. Everett, G. M. Fleming, and E. A. Smith, 2002: Plans for Global Precipitation Measurement ground validation. *Proc. Int. Geoscience Rem. Sens. Symp.*, Toronto, 24-28 June.
- Calheiros, R. V., and I. Zawadzki, 1987: Reflectivity rain-rate relationship for radar hydrology and Brazil. *J. Clim. Appl. Meteor.*, **26**, 118-132.
- Conner, M. D., and G. W. Petty, 1998: Validation and intercomparison of SSM/I rain rate retrieval methods over the continental United States. *J. Appl. Meteor.*, **37**, 679-700.
- Davolio, S., and A. Buzzi, 2002: Assimilation of satellite precipitation data into a LAM. *Int. Conf. on Quantitative Precipitation Forecasting*, Royal Meteor. Soc., 2-6 September, Reading, England.
- Ebert, E. E., and M. J. Manton, 1998: Performance of Satellite Rainfall Estimation Algorithms during TOGA COARE. *J. Atmos. Sci.*, **55**, 1537-1557.
- Ferraro, R. R., 1997: Special sensor microwave imager derived global rainfall estimates for climatological applications. *J. Geophys. Res.*, **102**, D14, 16715-16735.
- , E. A. Smith, W. Berg, and G. J. Huffman, 1998: A screening methodology for passive microwave precipitation retrieval algorithms. *J. Atmos. Sci.*, **55**, 1583-1600.
- Fleming, G. F., 2002: Requirements for Global Precipitation Measurement. *Proc. Int. Geoscience Rem. Sens. Symp.*, Toronto, 24-28 June.
- Greco, M., and E. N. Anagnostou, 2001: Overland precipitation estimation from TRMM passive microwave observations. *J. Appl. Meteor.*, **40**, 1367-1380.
- , ———, and R. F. Adler, 2000: Assessment of the use of lightning information in satellite infrared rainfall estimation. *J. Hydrometeor.*, **1**, 211-221.

- Grose, A., E. A. Smith, H.-S. Chung, M.-L. Ou, B.-J. Sohn, and F. J. Turk, 2002: Possibilities and limitations for QPF using nowcasting methods with infrared geosynchronous satellite imagery. *J. Appl. Meteor.*, **41**, 763-785.
- Hollinger, J. P., J. L. Peirce, and G. A. Poe, 1990: SSM/I instrument evaluation. *IEEE Trans. Geosci. Rem. Sens.*, **28(5)**, 781-790.
- Hou, A. Y., S. Zhang, A. da Silva, W. Olson, C. Kummerow, and J. Simpson, 2001: Improving global analysis and short-range forecast using rainfall and moisture observations derived from TRMM and SSM/I passive microwave sensors. *Bull. Amer. Meteor. Soc.*, **81**, 659-679.
- Huffman, G. J., R. F. Adler, P. A. Arkin, A. Chang, R. R. Ferraro, A. Gruber, J. Janowiak, A. McNab, B. Rudolf, and U. Schneider, 1997: The Global Precipitation Climatology Project (GPCP) combined precipitation dataset. *Bull. Amer. Meteor. Soc.*, **78**, 5-20.
- Imaoka, K., and R. W. Spencer, 2000: Diurnal variation of precipitation over the tropical oceans observed by TRMM/TMI combined with SSM/I. *J. Climate*, **13**, 4149-4158.
- Kidd, C., D. Kniveton, and E.C. Barrett, 1998: The advantages and disadvantages of statistically-derived, empirically-calibrated passive microwave algorithms for rainfall estimation. *J. Atmos. Sci.*, **55**, 1576-1582.
- Krishnamurti, T. N., S. Surendan, D. W. Shin, R. J. Correa-Torres, T. S. Vijaya Kumar, E. Williford, C. Kummerow, R. F. Adler, J. Simpson, R. Kakar, W. S. Olson, and F. J. Turk, 2001: Real time multianalysis/multimodel superensemble forecasts of precipitation using TMI and SSM/I products. *Mon. Wea. Rev.*, **129**, 2861-2883.
- Kuligowski, R. J., 2002: A self-calibrating real-time GOES rainfall algorithm for short-term rainfall estimates. *J. Hydrometeorology*, **3**, 112-130.
- Kummerow, C. D., Y. Hong, W. S. Olson, S. Yang, R. F. Adler, J. McCollum, R. Ferraro, G. Petty, D. B. Shin, and T. T. Wilheit, 2001: The evolution of the Goddard Profiling Algorithm (GPROF) for rainfall estimation from passive microwave sensors. *J. Appl. Meteor.*, **40**, 1801-1817.
- , and coauthors, 2000: The status of the Tropical Rainfall Measuring Mission (TRMM) after two years in orbit. *J. Appl. Meteor.*, **39**, 1965-1982.
- , W. Barnes, T. Kozu, J. Shiue, and J. Simpson, 1998: The Tropical Rainfall Measuring Mission (TRMM) sensor package. *J. Atmos. Oceanic Technol.*, **15**, 809-817.
- Levizzani, V., F. Porcu, F. S. Marzano, A. Mugnai, E. A. Smith, and F. Prodi, 1996: Investigating a SSM/I microwave algorithm to calibrate Meteosat infrared instantaneous rain rate estimates. *Meteorol. Appl.*, **3**, 5-17.
- , P. Bauer, A. Buzzi, D. E. Hinsman, A. Khain, C. Kidd, F. S. Marzano, F. Meneguzzo, A. Mugnai, J. P. V. Poyares Baptista, F. Prodi, J. F. W. Purdom, D. Rosenfeld, J. Schmetz, E. A. Smith, F. Tampieri, F. J. Turk, and G. A. Vicente, 2001: EURAINSAT: European satellite rainfall analysis and monitoring at the geostationary scale. *Prepr. 11th Conf. Satellite Meteor. Ocean.*, AMS, Madison, WI, 15-18 Oct., 650-653.
- , F. Torricella, R. Amorati, F. J. Turk, F. Meneguzzo, and P. P. Alberoni, 2002: MW-IR satellite rainfall measurements over northern Italy for the monitoring of heavy rains *Int. Conf. on Quantitative Precipitation Forecasting*, Royal Meteor. Soc., 2-6 September, Reading, England.
- Marzano, F. S., M. Palmacci, D. Cimini, and F. J. Turk, 2002: Statistical integration of satellite passive microwave and infrared data for high-temporal sampling retrieval of rainfall. *Proc. Int. Geosci. Rem. Sens. Symp. (IGARSS-2002)*, Toronto.
- McCollum, J. R., A. Gruber, and M. B. Ba, 2000: Discrepancies between gauges and satellite estimates of rainfall in equatorial Africa. *J. Appl. Meteor.*, **39**, 666-679.
- Miller, S. W., P. A. Arkin, and R. Joyce, 2001: A combined microwave/infrared rain rate algorithm. *Int. J. Remote Sensing*, **22**, 3285-3307.
- Morales, C., and E. N. Anagnostou, 2003: Extending the capabilities of rainfall estimation from satellite infrared via long-range lightning network observations. *J. Hydrometeorology*, **4**, 141-159.
- Oh, H.-J., B.-J. Sohn, E. A. Smith, F. J. Turk, A.-S. Seo, and H.-S. Chung, 2002: Validating infrared-based rainfall retrieval algorithms with 1-minute spatially dense raingauge measurements over the Korean peninsula. *Meteor. Atmos. Physics*, **79**, in press.
- Schmetz, J., P. Pili, S. Tjemkes, D. Just, J. Kerkmann, S. Rota, and A. Raiter, 2002: An introduction to Meteosat Second Generation (MSG). *Bull. Amer. Meteor. Soc.*, **83**, 977-992.

- Smith, E. A., and coauthors, 1998: Results of WetNet PIP-2 project. *J. Appl. Meteor.*, **55**, 1483-1536.
- , J. Adams, P. Baptista, D. Everett, M. Flaming, Z. Haddad, T. Iguchi, E. Im, and C. Kummerow, 2001: Optimizing orbit-instrument configuration for the Global Precipitation Mission (GPM) satellite fleet. *Proc. Int. Geosci. Rem. Sens. Symp. (IGARSS-2001)*, July 9-13, Sydney, Australia.
- Soman, V. V., J. B. Valdes, and G. R. North, 1995: Satellite sampling and the diurnal cycle statistics of Darwin rainfall data. *J. Appl. Meteor.*, **34**, 2481-2490.
- Spencer, R. W., H. M. Goodman, and R. E. Hood, 1989: Precipitation retrieval over land and ocean with the SSM/I: Identification and characteristics of the scattering signal. *J. Atmos. Ocean. Tech.*, **6**, 254-273.
- Todd, M. C., C. Kidd, D. Kniveton, and T. J. Bellerby, 2001: A combined satellite infrared and passive microwave technique for estimation of small-scale rainfall. *J. Atmos. Oceanic Technol.*, **18**, 742-755.
- Turk, F. J. G. Rohaly, J. Hawkins, E. A. Smith, A. Grose, A., F.S. Marzano, A. Mugnai, and V. Levizzani, 2000: Analysis and assimilation of rainfall from blended SSM/I, TRMM and geostationary satellite data. *Prepr. 10<sup>th</sup> AMS Conf. Sat. Meteor. and Ocean.*, 9-14 January, Long Beach, CA., 66-69.
- Vicente, G. A., 1994: *Hourly retrieval of precipitation rate from the combination of passive microwave and infrared satellite measurements*. Ph.D. dissertation, Univ. of Wisconsin, Madison, WI, USA.
- , J. C. Davenport, and R. A. Scofield, 2002: The role of orographic and parallax correction on real time, high resolution satellite rain rate observation. *Int. J. Rem. Sens.*, **23**, 221-230.
- Vivekanandan, J., F. J. Turk, and V. N. Bringi, 1991: Ice water path estimation and characterization using passive microwave radiometry. *J. Appl. Meteor.*, **30**, 1407-1421.
- Weng, F., R. R. Ferraro, and N. C Grody, 2002: Advances in AMSU non-sounding products. *Proc. 12<sup>th</sup> Int. TOVS Study Conf.*, 26 February-12 March, Lorne, Victoria, Australia.
- Weymouth, G., G. A. Mills, D. Jones, E. E. Ebert, and M. J. Manton, 1999: A continental-scale daily rainfall analysis system. *Australian Meteor. Mag.*, **48**, 169-179.